NeuroImage 245 (2021) 118636

Contents lists available at ScienceDirect

NeuroImage

journal homepage: www.elsevier.com/locate/neuroimage

How recent learning shapes the brain: Memory-dependent functional reconfiguration of brain circuits

Roberta Passiatore[a,b,#], Linda A. Antonucci[a,c,#], Sabine Bierstedt[d], Manojkumar Saranathan[e], Alessandro Bertolino[a], Boris Suchan[d], Giulio Pergola[a,f,*]

[a] Department of Basic Medical Sciences, Neuroscience and Sense Organs, University of Bari Aldo Moro, Piazza Giulio Cesare, 11, Bari, IT 70124, Italy
[b] Tri-Institutional Center for Translational Research in Neuroimaging and Data Science (TReNDS), Georgia State University, Georgia Institute of Technology, Emory University, Atlanta GA 30303, United States
[c] Department of Education, Psychology and Communication Science, University of Bari Aldo Moro, Bari, IT 70121, Italy
[d] Institute of Cognitive Neuroscience, Clinical Neuropsychology, Ruhr University Bochum, Bochum, DE 44801, Germany
[e] Department of Medical Imaging, University of Arizona, Tucson AZ 85724, United States
[f] Lieber Institute for Brain Development, Johns Hopkins Medical Campus, Baltimore MD 21205, United States

ARTICLE INFO

Keywords:
Learning
Episodic memory
Functional connectivity
Independent component analysis
System configuration
Resting state

ABSTRACT

The process of storing recently encoded episodic mnestic traces so that they are available for subsequent retrieval is accompanied by specific brain functional connectivity (FC) changes. In this fMRI study, we examined the early processing of memories in twenty-eight healthy participants performing an episodic memory task interposed between two resting state sessions. Memory performance was assessed through a forced-choice recognition test after the scanning sessions.

We investigated resting state system configuration changes via Independent Component Analysis by cross-modeling baseline resting state spatial maps onto the post-encoding resting state, and post-encoding resting state spatial maps onto baseline.

We identified both persistent and plastic components of the overall brain functional configuration between baseline and post-encoding. While FC patterns within executive, default mode, and cerebellar circuits persisted from baseline to post-encoding, FC within the visual circuit changed. A significant session × performance interaction characterized medial temporal lobe and prefrontal cortex FC with the visual circuit, as well as thalamic FC within the executive control system.

Findings reveal early-stage FC changes at the system-level subsequent to a learning experience and associated with inter-individual variation in memory performance.

1. Introduction

Learning novel information is a flexible process consisting of encoding of memories for subsequent retrieval (Dudai et al., 2015). This flexible behavioral system is supported by brain functional changes underlying storage and strategic access to stored information. Brain connectivity changes occur both at synaptic and system-level (Olsen and Robin, 2020). At the synaptic level, learning-dependent plasticity involves the reinforcement of neuronal connections (Dudai, 2004). By contrast, system level plasticity refers to the relationship between functional brain systems supporting memory, including circuits subserving attention, salience, default mode, and long-term memory (Frankland and Bontempi, 2005).

Newly encoded memories are initially dependent on the hippocampus and surrounding medial temporal lobe (MTL) regions (Alvarez and Squire, 1994). While some memories decay rapidly, others are processed and become gradually integrated within wider neocortical circuits over time (Frankland and Bontempi, 2005; Nadel and Moscovitch, 1997). This mechanism relies on the communication between the hippocampus and other brain regions, such as parahippocampal gyrus, prefrontal cortex, and thalamus (Pergola and Suchan, 2013), whose connections underly post-encoding memory processing. Thus, investigating circuit-level functional connectivity (FC) between episodic memory regions shortly after encoding offers an opportunity to study the early stage of memory traces in the human brain.

* Corresponding author.
E-mail address: giulio.pergola@uniba.it (G. Pergola).
# These authors contributed equally.

https://doi.org/10.1016/j.neuroimage.2021.118636.
Received 23 May 2021; Received in revised form 20 September 2021; Accepted 5 October 2021
Available online 9 October 2021.

The involvement of FC pattern changes across spatially distributed circuits in cognition has already been demonstrated within cross-sectional frameworks in several domains, i.e., visual, working memory, recognition memory, and strategic attention tasks when comparing task-evoked FC with resting state (Bassett et al., 2011; Cohen and D'Esposito, 2016; Sambataro et al., 2010b, 2012; Yue et al., 2017). For example, Sambataro et al. (2012) showed decreased Independent Component Analysis-based [ICA, Calhoun et al. (2001)] FC patterns within a network including prefrontal, parietal and occipital cortices as function of memory abilities during normal aging. The authors jointly analyzed an episodic memory and a working memory task showing that greater memory performance was associated with lower FC between prefrontal, parietal and occipital cortices, and higher task-specialization across the fronto-parietal-visual circuit. Moreover, previous evidence highlighted that the spatial configuration of FC patterns during resting state is highly similar to the FC spatial configuration of the same circuits, in the same individuals, during the performance of multiple cognitive tasks, i.e., emotional, relational memory, language, gambling, motor, social, and working memory tasks (Cole et al., 2014). However, within- and between-circuit FC patterns change in key-regions for episodic memory as a function of task demands, even if the circuit configuration remains the same. Cole et al. (2014) showed that frontal and parietal cortical regions changed their functional connections, being initially connected with default mode circuit during resting state and shifting to the visual circuit during active task conditions. Interestingly, fronto-parietal FC changes were configured into distinct patterns as a function of task demand and domain, to the extent that fronto-parietal FC could be distinctive for specific task states (Cole et al., 2013).

Overall, this body of evidence suggests that brain configurations are flexible, as they flexibly adapt their within- and between-circuit properties to the demands, domains, and properties of a task. On this basis, we hypothesize that the overall learning experience may perturb previously stable circuit configurations already few minutes after the exposure to new stimuli. If so, a change in FC patterns would be potentially detectable already after a short period of time.

Neuroimaging studies investigating FC changes between pre-encoding (i.e., baseline) and post-encoding resting state sessions have reported FC pattern changes characterizing the shift from one phase to the other. For example, Tambini et al. (2010) showed that hippocampus and lateral occipital cortex (involved in visual processing) change their connectivity as a function of visual memory task demands immediately after encoding. These regions had higher FC after encoding relative to baseline when considering object-face encoding (but not scene-face pairs). A later study explored the inter-individual variation component of early memory traces showing that post-encoding visual cortex functional plasticity correlated with individual memory performance (Brodt et al., 2018). This study supported a visual cortex involvement in early-stage information retention after episodic memory encoding. Within the theoretical framework outlined above, these findings may be interpreted as reflecting FC changes between hippocampus and cortical regions occurring immediately (Tambini et al., 2010) and one hour (Brodt et al., 2018) after encoding. Consistently, using an analogous repeated resting state paradigm, Wagner et al. (2019) reported that FC between MTL and cortical regions is mediated by the thalamus comparing baseline and a subsequent post-encoding resting state sessions. FC predicted memory scores collected 48 h after the scanning session.

In summary, these studies highlight that FC pattern changes mirroring the course of episodic memory traces exhibit early involvement of the visual cortex, and a more far-reaching involvement of the thalamus, in interaction with the MTL, with some evidence that these pattern changes are related with inter-individual performance variation. This evidence suggests that the brain circuit supporting memory not only relies on FC between localized memory key regions, but rather points to the relevance of wider, system-level spatially distributed FC changes (i) which are subsequent to memory encoding, and (ii) which take place shortly after the conclusion of the learning experience. Thus, an outstanding question is to what extent inter-individual variation in memory performance is associated with early-stage FC changes at system-level and which brain circuits are involved.

We aimed to investigate how flexible interactions between localized key regions and whole-brain configuration support memory. More specifically, since memory performance varies between individuals, we aimed at investigating how FC between memory key regions, such as MTL and thalamus, and multiple cortical circuits is associated with individual memory performance. Our main hypotheses were (i) that brain system configuration undergoes spatial changes characterizing the shift from a baseline to a post-encoding condition, (ii) that the FC of memory key regions with these reconfigured brain circuits change after learning, and (iii) that such system-level and regional-level changes may be associated with individual performance.

We examined whole-brain FC via ICA (Calhoun et al., 2001) rather than functional coupling between preselected regions, employing high spatial resolution fMRI to enhance anatomic granularity. We tested the hypothesis that FC changes follow episodic memory task performance at the whole-brain level by means of correlations between session-specific Independent Components (IC), and the session × performance interaction on FC between localized episodic memory key regions and whole-brain circuits as a function of individual memory performance.

Here, we show time and task-dependent FC changes at the system and regional level in relation to early memory processes, which could explain part of the inter-individual variability in memory performance.

2. Materials and methods

2.1. Participants

We recruited 36 healthy adults for a fMRI study. All participants had normal or corrected-to-normal vision. Vision correction during MRI was achieved via contact lenses or MRI compatible glasses. No individual had a history of drug or alcohol abuse within the last 6 months, head trauma with loss of consciousness, or any clinically relevant medical condition. For each participant, handedness was assessed through the Edinburgh Handedness Inventory (EHI, Oldfield, 1971). The study was approved by the Ethics Committee of the Faculty of Medicine of the Ruhr-Universität Bochum. All participants gave written informed consent before participating, following the Declaration of Helsinki. A total of 28 participants were included in the final sample (mean age ± SD = 26 ± 3 years; gender ratio, m: f = 9:19; mean handedness ± SD = 0.89 ± 0.11) following exclusion criteria described in detail in the Supplementary materials, Section 1. One ambidextrous participant (EHI = 0.2) was excluded to reduce heterogeneity for laterality (Ferrucci et al., 2013). Five participants did not complete the protocol due to technical failure during data collection and two more were excluded because of data artifacts and excessive motion during the acquisition.

2.2. Experimental procedure

The experimental procedure is outlined in Fig. 1a. The experiment involved a pre-scanning practice, during which participants completed a training block with stimuli not used in the following episodic memory task. The fMRI scanning was composed of multiple sessions, i.e., acquisitions within a single scanning period including (1) resting state (baseline), (2) four experimental blocks of the episodic memory task, and (3) a second resting state (post-encoding) following the episodic memory task when post-encoding memory process is presumably taking place. During each resting state session, participants were instructed to remain awake, with eyes open and to fixate the crosshair in the middle of a black screen (Damoiseaux et al., 2006; Greicius et al., 2003). Each resting state session lasted 8 min.

During the episodic memory task session, each participant performed four experimental blocks. Each block included an encoding, a delay,

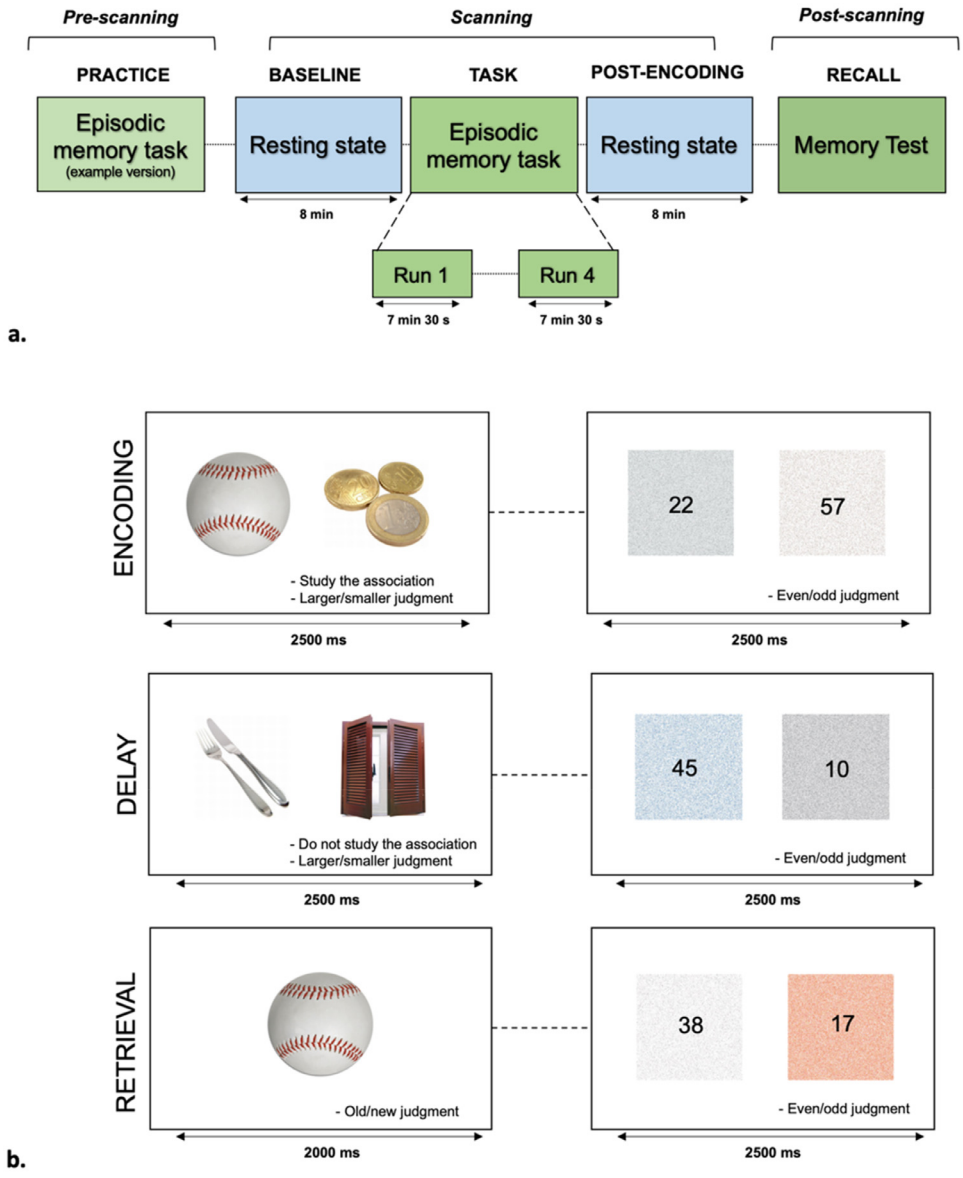

Fig. 1. Experiment design. (a) General experimental procedure outline. (b) The episodic memory task.

and a retrieval condition. During encoding, participants were explicitly asked to study the association between object-object picture pairs projected on the screen and indicate which object was larger/smaller in real life. During the delay, unstudied object-object picture pairs were presented while participants indicated which object was larger in reality, but not memorizing the association between picture pairs. During retrieval, participants were asked to perform an old/new judgment while single pictures were presented on the screen, of which 2/3 were studied during the encoding conditions and the remaining were completely new. Interleaved with the task trials, participants were presented with pairs of two-digit numbers, each placed at the center of scrambled pictures pairs, and performed an odd/even judgment. This condition was designed to reset the BOLD signal in the MTL to baseline, enhancing task-related activity (Stark and Squire, 2001). The whole episodic memory task session lasted approximately 30 min. The episodic memory task is depicted in Fig. 1b. For a detailed description of the stimuli selection and experimental procedure, see Supplementary materials, Sections 2 and 3.

After the scan, participants performed a self-paced forced-choice memory test outside the scanner. They were informed about the subsequent memory test before entering the scanner. Participants were again presented with all the pictures they had correctly indicated as 'old' during the item retrieval (Hits), one by one. Upon the presentation of the picture, participants rated their confidence in recalling the association with a 4-point Likert scale, with 1 representing certain recall, and 4 representing guesses. Afterwards, two additional pictures were presented on the computer screen, i.e., the paired picture during the encoding on one side and one of the pictures shown during the delay (foil) on the other. Participants were asked to select which picture had been presented with the cue during the encoding.

2.3. Behavioral analysis

We classified performance based on responses during the retrieval phase of the episodic memory task session and the subsequent memory test. Correct recall might indicate an accurate response or a correct guess, given the forced choice framing of our test (Kareev and Trope, 2011). To reduce this potential problem, for subsequent memory trial classification we included the "guess option" (confidence rating=4). Specifically, we determined:

- the Hit count, reflecting the successful recognition during retrieval of pictures studied during encoding

Table 1
Overview of the classification of the behavioral performance during the episodic memory task session during fMRI. The classification of Hits during the subsequent memory test is shown in italic. Abbreviations: CR = Correct Rejection; FA = False Alarm; NR = No Response.

Categories	Description
Hits	Responses successfully classifying an old item as old
H^+	*Hits followed by correct recall of the paired picture*
H^-	*Hits followed by incorrect recall of the paired picture, with confidence ratings between 1 and 3*
H^0	*Hits followed by correct or incorrect recall of the paired picture, with confidence ratings equal to 4*
CR	Responses successfully classifying a new item as new
FA	Responses incorrectly classifying a new item as old
Misses	Responses incorrectly classifying an old item as new
NR	The subject failed to respond within the given time
Num	Control - Even/Odd judgment

- the H^+ count, representing hits with subsequent recall of paired pictures
- the H^-count, representing hits with incorrect subsequent recall, with confidence ratings between 1 and 3
- the H^0 count, representing the correct or incorrect subsequent recall with confidence ratings equal to 4, thus allowing us to remove guessed responses from the computation of H^+, since the task implied a forced choice
- the correct rejections count, representing the successful classification of a new item as such.

We also determined the reaction times (RT) parsed by response type from the retrieval session. Table 1 summarizes response classification and the RT indices.

To assess memory performance, we compared the rate of successful subsequent memory (i.e., the percentage of correctly recalled pictures [H^+/Hits]) with the rate of unsuccessful subsequent memory (i.e., the percentage of incorrect recalled pictures with confidence ratings 1–3 and guesses [(H^-+H^0)/Hits]). We discriminated unsuccessful subsequent memory in the two categories within fMRI to obtain greater granularity, but pooled H^- and H^0 in the behavioral assessment to compensate for differences in participants' response strategies. We assessed successful group-level subsequent memory performance by a paired *t*-test. Given that chance performance is 50%, our null hypothesis was H^+ rate = (H^-+H^0 rate).

Furthermore, a cued recall index was computed as the ratio between H^+ and the number of valid trials recorded during encoding [H^+/(trials – no responses)] (Pergola et al., 2012) to quantify the successful subsequent memory performance independent of recognition performance variation between participants. The cued recall index was included as covariate of interest in further second-level analysis conducted on resting state data (see Section 2.8). Shapiro-Wilk tests on performance indices served to test for deviations from the normal distribution.

Finally, we analyzed performance speed in terms of RT by means of paired t-tests. We tested the effect of both response type (Hits vs CR) and subsequent memory condition (H^+; averaged H^- and H^0) on RT. Statistical significance was set at α<0.05.

2.4. Structural and functional MRI data acquisition and processing

Structural and functional images were acquired with a Philips Achieva 3 Tesla scanner.

A T1-weighted axial sequence (voxel size = 0.83 × 0.83 × 0.9 mm) was obtained at the beginning of the scanning session. Between the second and the third block of the episodic memory task, a second localizer and a T2-weighted axial sequence (0.45 × 0.45 × 4 mm) were acquired to allow adjusting the scanning window in case the participant moved. Individual structural images were preprocessed with the Statistical Parametric Mapping (SPM) version 12 (http://www.fil.ion.ucl.ac.uk/spm) and the Computational Anatomy Toolbox (CAT12, http://dbm.neuro.uni-jena.de/cat/). We checked the quality of individual segmented maps via visual inspection. Finally, the Parallel Build Template function implemented in ANTs (Avants et al., 2009) generated a sample-defined high-resolution template. See Supplementary Materials, Section 4 for acquisition and preprocessing details.

Resting state and episodic memory task fMRI data were acquired using echo-planar imaging (EPI) sequence (resting state sequence characteristics: TR = 2500 ms; flip angle = 90°; 39 contiguous axial slices; voxel size = 1.44 × 1.44 × 3.2 mm; task sequence characteristics: TR = 2500 ms; flip angle = 70°; 29 axial slices; voxel size = 1.5 × 1.5 × 2 mm, slice gap = 0.4 mm). SPM12 was used to analyze functional data. Functional images were reoriented to the anterior commissure-posterior commissure (AC-PC) line with the origin in the AC. Then, they were corrected for differences in slice acquisition timing, aligned across both sessions, and unwarped. Datasets were inspected to check for excessive motion, which represented an exclusion criterion (>2 mm in translation and 1.5° in rotation). We also computed a measure of the movement of the head from one frame to the next during acquisition, i.e., the Frame-wise Displacement (FD). We set the acceptable FD threshold according to previously published reports [FD<0.05 (Power et al., 2012)]. Additionally, twenty-four motion parameters (Friston, 2003), as well as WM and CSF mean signals were regressed out to limit the effect of motion on connectivity estimates. Then, images were spatially registered to the individual structural image and spatially normalized to 2 mm isotropic (down-sampling to 8mm^3 from the original 6.6 mm^3) into the sample-defined common space through the Symmetric Normalization function implemented in ANTs. Functional images were visually inspected and spatially smoothed (6-mm Gaussian filter). A GLM approach was used to estimate parameter values for task events. Task events were assigned to the stimulus onset of each trial and convolved with canonical hemodynamic response function (HRF) implemented in SPM (see Supplementary materials, Section 5 for preprocessing details). As a sanity check, we investigated brain activation elicited by the fMRI episodic memory task. This analysis was performed to ensure that the conditions of the episodic memory task were associated with group-level brain activation consistent with previously established episodic memory FC patterns (Jeong et al., 2015; Moscovitch et al., 2016). First- and second-level fMRI analysis procedures and results are described in Supplementary materials, section 6.

2.5. Baseline and post-encoding resting state system configuration analyses

To investigate resting state session-specific FC features at the system level, spatial group ICA (Calhoun et al., 2001) was implemented by taking as input participant's resting state data separately for each resting state session (baseline and post-encoding). To obtain individual FC maps, the individual-level ICs were estimated for each resting state session (Fig. 2 Step 1). We used the fastICA algorithm (Hyvarinen, 1999), implemented in the GIFT v4.0a toolbox (https://trendscenter.org/software/gift/). See Supplementary materials, section 7 for further details.

The estimated ICs were screened for goodness and reliability based on visual inspection and the Index of quality (Iq), a measure of component stability (Antonucci et al., 2019; Himberg et al., 2004). We considered ICs with Iq index>0.7 to be reliable and stable (Ma et al., 2011). To select the components of interest (COIs) for further investigations, we performed spatial correlations between every IC spatial map and, separately, GM, WM, and CSF templates. We considered ICs featuring IC~GM correlation with R^2>0.02, IC~WM correlation with R^2<0.02, and IC~CSF correlation with R^2<0.05 as suitable for further analyses, following published procedures (Kim et al., 2009; Sambataro et al., 2010a). Movement–related ICs were excluded considering R^2>0.05 between the IC individual loadings and the Frame-wise Displacement (Power et al., 2012). Furthermore, we considered only ICs in which the

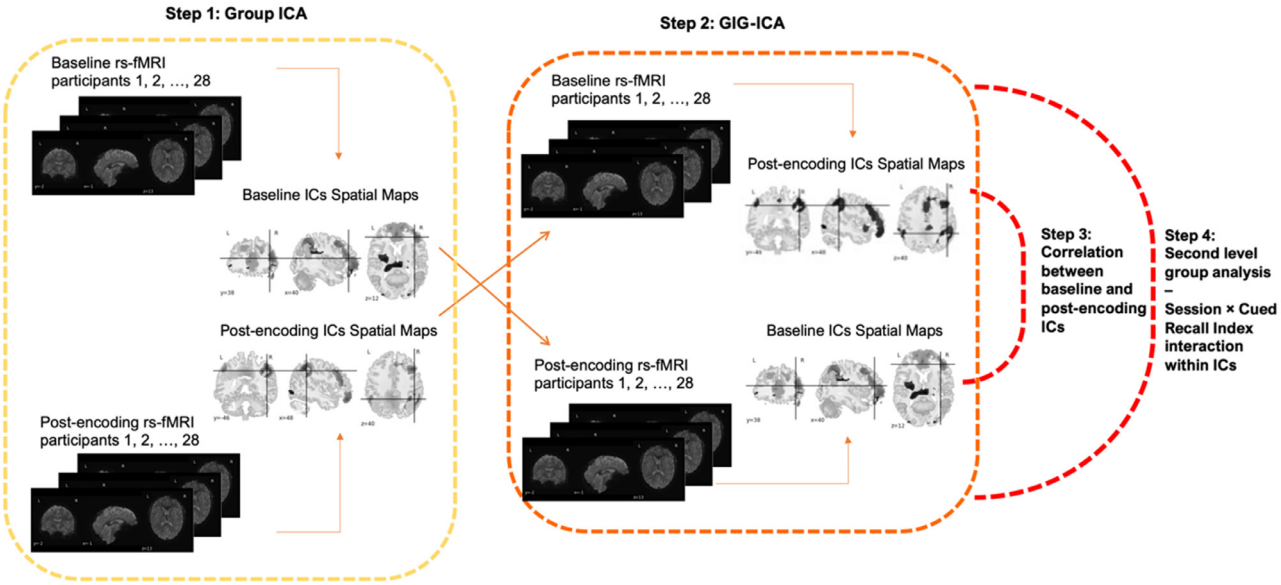

Fig. 2. The resting state system configuration analysis pipeline. Abbreviations: IC=Independent Component; ICA=Independent Component Analysis; GIG-ICA= Group Information Guided ICA.

amount of GM estimate was higher than the amount of WM estimate (Supplementary materials, section 7). To anatomically and functionally label the areas included in each COI, we determined the degree of overlap between each COI and a published template defining Large Scale functional spatial maps (Iraji et al., 2019) through spatial correlations (R^2>0.05) (Allen et al., 2011).

2.6. Forward and backward investigation of system reconfiguration between baseline and post-encoding resting state sessions

To investigate the session × performance interaction, we used a bidirectional approach useful to picture FC changes in a full temporal perspective. The previously defined COI maps, i.e., the whole-brain information captured by standard group ICA for one resting state session, were used as a reference to estimate individual COI loadings onto the other resting state session employing the GIG-ICA algorithm (Du and Fan, 2013) (Fig. 2 Step 2). Specifically, we spatially constrained post-encoding scans into baseline COI spatial maps (Forward ICA). This procedure investigated the modification in terms of configuration of baseline ICs (i.e., independent of the task, by definition) after the performance of the episodic memory task. In the opposite direction, we spatially constrained baseline scans into the post-encoding COI spatial maps (Backward ICA). This procedure estimates the brain configuration before the performance of the episodic task within post-encoding ICs (i.e., whose ICA-based separation is potentially affected by task performance).

2.7. Second level resting state system reconfiguration and FC patterns analysis

To assess whether the same system configuration persisted from baseline to post-encoding and how ICs changed after the episodic memory task, we tested the similarity between baseline estimated COIs and post-encoding estimated COIs (Fig. 2 Step 3). COIs were deemed similar when their voxel-wise loading correlation R^2>=0.1 (Antonucci et al., 2019, 2016). To characterize the association of the FC patterns of each circuit with memory performance, we calculated the correlation between each COI individual loadings and the cued recall index (R^2>=0.1). Finally, to define the regional involvement in circuit reconfiguration, we tested the session × performance interaction through SPM Flexible Factorial. We separately considered the individual loadings of the estimated COIs on baseline resting state scans and the corresponding constrained post-encoding individual loadings (backward ICA) as repeated measure. Vice-versa, we considered the individual loadings of the estimated COIs on post-encoding resting state scans and the corresponding constrained baseline individual loadings (forward ICA) as repeated measure (Fig. 2 Step 4). We included both persistent and non-persistent COIs separately for each session. Age, gender, and handedness were used as nuisance covariates. We used TFCE to correct statistics for multiple comparisons (TFCE-FWE<0.05, Supplementary materials, section 8).

3. Results

3.1. Behavioral analysis

Behavioral performance collected during the retrieval phase and the subsequent memory test is shown in Table 2. The overall rate of successful encoded trials [Hits] averaged 86% and did not significantly deviate from the normal distribution (Shapiro-Wilk test, $p = 0.3$). The rate of successful subsequent memory [H^+/Hit] averaged 60% and did not significantly deviate from the normal distribution (Shapiro-Wilk test, $p = 0.7$). Subsequent memory performance was above chance [paired t-test, $t(27) = 2.44$, $p = 0.02$]. Individual cued recall rate (rate of recalled association over the total number of trials) ranged between 18% and 91% without significantly deviating from the normal distribution (Shapiro-Wilk test, $p = 0.5$).

Paired t-tests across episodic memory task fMRI sessions conducted on RT revealed a significant effect of response type [$t(27) = -12.47$, $p = 0.0001$], with faster correct rejections than Hit responses. However, within Hits, RTs were shorter with successful subsequent memory (H^+), compared with the unsuccessful subsequent memory (H^-+H^0) [$t(27) = 5.52$, $p = 0.0001$].

3.2. Baseline and post-encoding resting state system configuration analysis

We estimated 25 ICs from the baseline ICA and five of them were selected following the previously described criteria (Fig. 3a and Table 3). The post-encoding resting state featured 24 ICs, of which 6 survived exclusion criteria (Fig. 3b and Table 3). Hereinafter, the apex 'b' denotes baseline COIs, while apex 'p' refers to post-encoding COIs.

Table 2
Behavioral performance during the episodic memory task. The behavioral performance of Hits which have been defined based on the response recorded during the subsequent memory test is shown in italic. Abbreviations: SD = Standard Deviation; RT = Reaction Time; H^+ = Complete recall; H^- = Partial Recall; H^0 = No recall; CR = Correct Rejection; FA = False Alarm; NR = No Response.

Categories	N Mean ± SD	Total N of trials	%mean ± SD	mean RT ± SD (ms)	RT min:max (ms)
Hits	68 ± 6	80	86.02 ± 7.6	837± 135	578:1043
H^+	40 ± 13	80	50.31 ± 16	*1099* ± 63	*889:1148*
H^-	22 ± 11	80	27.72 ± 14.7	*1064* ± 62	*846:1186*
H^0	6 ± 7	80	7.99 ± 9.97	*811* ± 238	*442:956*
CR	36 ± 2	48	76.56 ± 5.54	1178± 59	925:1245
FA	2 ± 2	48	5.65 ± 4.93	537 ± 739	2320:227
Misses	10 ± 6	80	12.09 ± 7.03	1394 ± 505	715:2427
NR	1 ± 2	128	0.94 ± 1.2	–	–

Table 3
Resting state circuits characteristics. Column 2, *Spatial map labeling:* spatial correlations between baseline and post-encoding COIs and previously published templates large-scale functional maps (Iraji et al., 2019). Column 3, *Association with performance*: correlations between individual connectivity loadings of both baseline and post-encoding and the cued recall index. Significance was set at $p<0.05$. The apex 'b' refers to baseline COIs, while apex 'p' refers to post-encoding COIs. Abbreviation: COI = Component of Interest.

Session	COIs	Spatial map labeling [R^2]	Association with performance [Person's r (FDR p-value)]
BASELINE	$COI1^b$	Executive Control Circuit = 0.3	0.4 (0.02)
	$COI2^b$	Posterior Default Mode Circuit = 0.1	0.1 (0.1)
	$COI3^b$	Primary Visual Circuit = 0.06	−0.05 (0.2)
	$COI4^b$	Cerebellar Circuit = 0.3	0.3 (0.1)
	$COI5^b$	Anterior Default Mode Circuit = 0.5	0.2 (0.1)
POST-ENCODING	$COI1^p$	Executive Control Circuit = 0.3	0.4 (0.03)
	$COI2^p$	Posterior Default Mode Circuit = 0.6	−0.05 (0.1)
	$COI3^p$	Primary Visual Circuit = 0.07	−0.4 (0.03)
	$COI4^p$	Cerebellar Circuit = 0.1	−0.3 (0.1)
	$COI5^p$	Salience Circuit = 0.1	−0.1 (0.1)
	$COI6^p$	Secondary Visual Circuit = 0.3	−0.1 (0.2)

We found that the default mode circuit configuration persisted from baseline to post-encoding resting state (R^2=0.61; p-value<0.0001; $COI2^b$ and $COI2^p$), and both COIs were uncorrelated with the cued recall index (respectively, Pearson's r = 0.1, p-value = 0.1, and Pearson's r = −0.05, p-value = 0.1). We found that the left insula FC patterns with the posterior default mode circuit was lower for best performers only during baseline (MNI coord: −40 −4 2; Fig. 4a and 4b), when constraining post-encoding scans into baseline COI spatial maps (forward ICA).

Also, the executive control circuit configuration persisted from baseline to post-encoding resting state (R^2 = 0.73; p-value<0.0001; $COI1^b$ and $COI1^p$). In this case, individual loadings of both COIs were positively associated with the cued recall index (respectively, Person's r = 0.4, p-value = 0.02, and Pearson's r = 0.4, p-value = 0.03). Within this circuit, the right thalamic connectivity was positively correlated with subsequent memory performance during post-encoding but negatively correlated during baseline (MNI coord: 18 −10 6; Fig. 4g and 4h), when constraining baseline scans into post-encoding COI spatial maps (backward ICA, Fig. 2). See Supplementary Materials, section 9 for further information.

A further association linked baseline and post-encoding cerebellar circuits (R^2 = 0.69; p-value<0.0001; $COI4^b$ and $COI4^p$), which were not associated with subsequent memory performance (respectively, Pearson's r = 0.3, p-value = 0.1 and Person's r = −0.3, p-value = 0.1). The persistence of these three circuits in terms of spatial configuration suggests that these circuits were highly reproducible within-participants across sessions.

Interestingly, we found that visual circuits are reconfigured from baseline to post-encoding resting state. Specifically, the baseline visual circuit ($COI3^b$) only partially overlapped with both the post-encoding cerebellar-visual circuit ($COI3^p$, R^2 = 0.1; p-value<0.0001) and the post-encoding visual circuit ($COI6^p$, R^2 = 0.1; p-value = 0.001), suggesting that this circuit underwent some degree of reconfiguration after the episodic memory task. There was no association between the baseline visual circuit and the cued recall index during baseline (Pearson's r = −0.05, p-value = 0.2), whereas only the post-encoding visual circuit ($COI6^p$) partially overlapping with the baseline visual circuit was also associated with the cued recall index (Pearson's r = −0.4, p-value = 0.03).

The session × performance interaction analysis revealed that the connectivity loadings of a cluster in the MTL (specifically located in the parahippocampal gyrus, MNI coord: −26 −44 −8; Figs. 4c and 4d) and of a cluster in BA9 were higher for best performers during baseline and not post-encoding (MNI coord: 50 26 26; Figs. 4e and 4f), when constraining post-encoding scans into baseline COI spatial maps (forward ICA, Fig. 2). On the other hand, the connectivity of the MTL cluster with the visual circuit was lower in best performers (MNI coord: 31 −34 −18; Figs. 4i and 4j), whereas BA10 connectivity within the same circuit was higher (MNI coord: 11 54 7; Figs. 4k and 4l) selectively during post-encoding, when constraining baseline scans into post-encoding COI spatial maps (backward ICA).

In summary, the forward/backward ICA results showed: (1) FC changes in a cluster located in the left insula within a default mode circuit showing persistency in terms of brain spatial configuration; (2) FC changes in a cluster located in the right thalamus within a stable executive control circuit, as a function of memory performance; (3) a shift in visual FC patterns from baseline to post-encoding; and (4) visual FC patterns changes with MTL and PFC as function of memory performance.

Additionally, the baseline anterior default mode circuit ($COI5^b$) failed to replicate during post-encoding and the post-encoding salience circuit ($COI5^p$) was not found during baseline. Fig. 5 illustrates the correlation between baseline COIs and post-encoding COIs and Fig. 6 shows the spatial overlap between stable baseline and post-encoding COIs.

4. Discussion

The present study aimed to investigate the early stage of episodic memory trace formation in terms of brain system configuration. We identified learning-related FC patterns changes within brain circuits shortly after the performance of an episodic memory task, which were

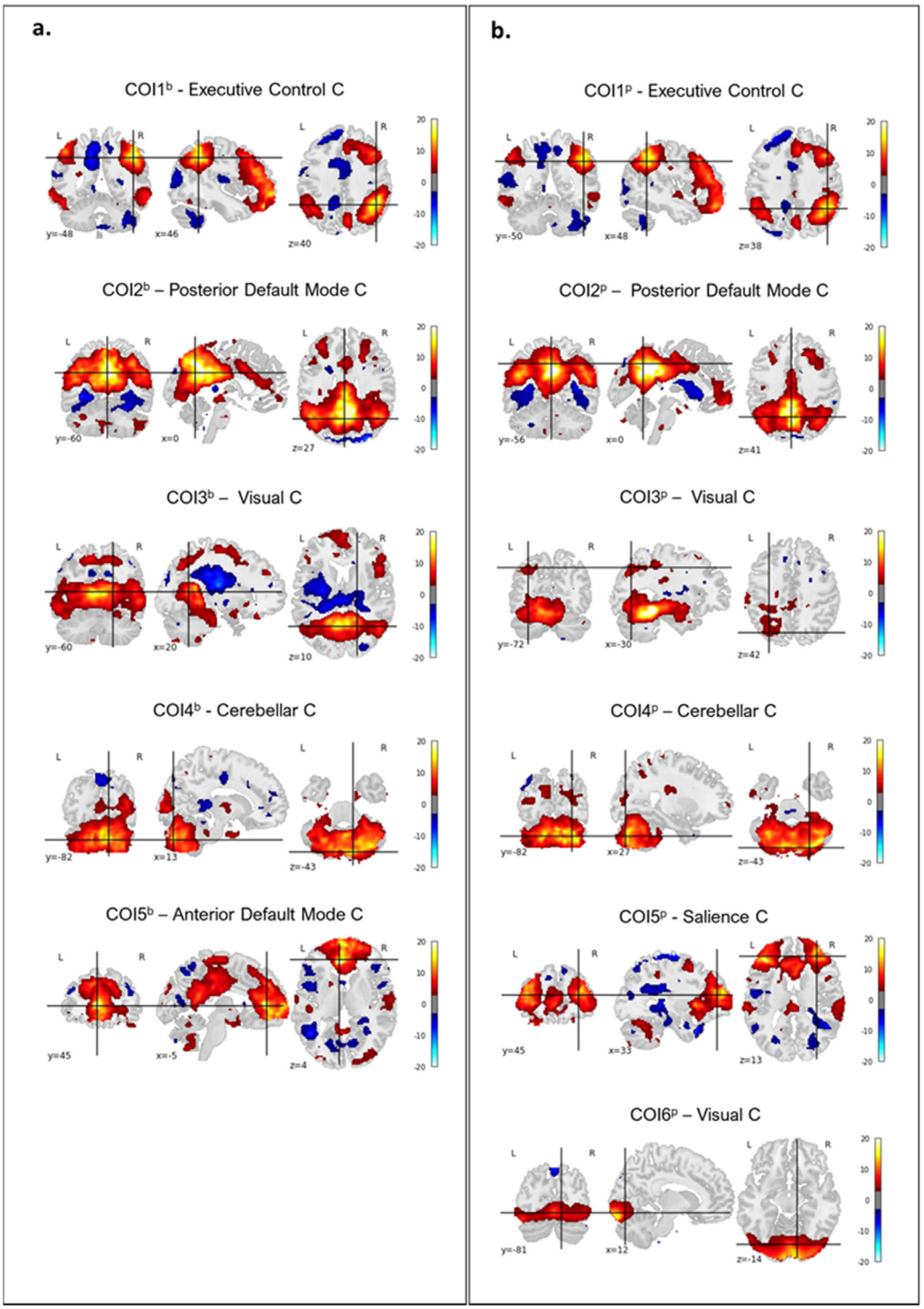

Fig. 3. Baseline and post-encoding circuits. (a) COIs spatial maps of the 5 brain-circuits obtained by ICA on baseline resting state fMRI (b) COIs spatial maps of the 6 brain-circuits obtained by ICA on post-encoding resting state fMRI. Spatial maps are plotted as z-scores and thresholded at $|Z|>3$. Abbreviations: COI=Component of Interest; the apex 'b' refers to baseline COIs, while apex 'p' refers to post-encoding COIs; *C*=Circuit.

associated with inter-individual variability in subsequent memory performance.

We investigated the association between memory performance and system configuration in both baseline and post-encoding resting state sessions. While configuration within executive, default mode, and cerebellar circuits persisted across sessions, the configuration of the visual circuit changed. This reconfiguration was compounded by a significant session × performance interaction on FC patterns of MTL and PFC with the visual circuits between sessions. Also, thalamic involvement with the executive control circuit varied in association with individual memory performance.

4.1. *Behavioral findings support task effectiveness*

Behavioral results suggested that the episodic memory task was able to capture inter-individual variability in terms of memory abilities that we summarize in the cued recall index. As previously reported, best performers made faster old/new decisions (Dewhurst et al., 2006;

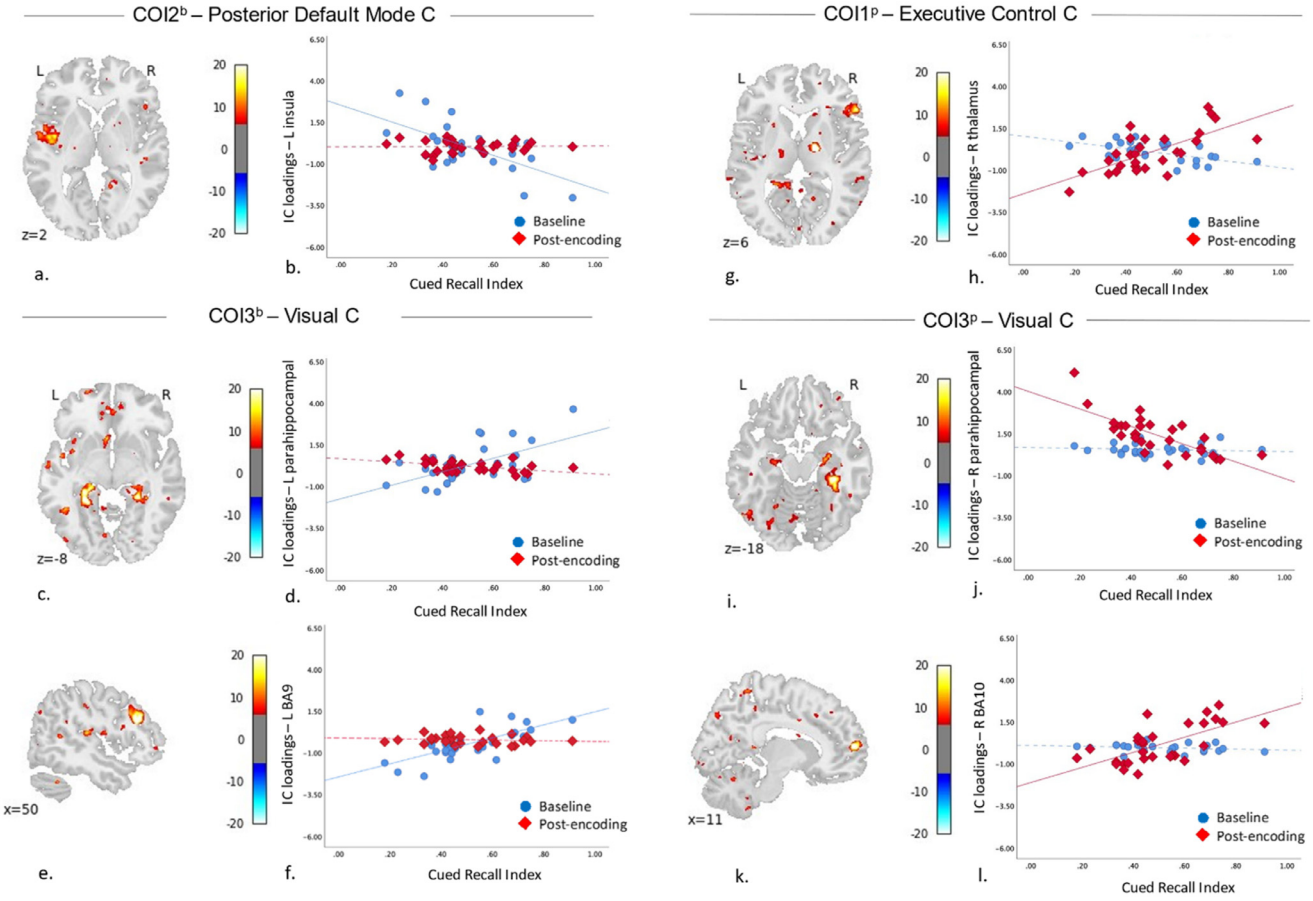

Fig. 4. Session × performance interactions. (a) Axial image of the session × performance interaction located in the left insula within the baseline Posterior default mode circuit. (b) Scatterplot of the interaction between the cued recall index and connectivity loadings of the cluster depicted in (a) and grouped by resting state sessions. (c) Axial image of the session × performance interaction located in the left parahippocampal gyrus with the baseline Primary visual circuit. (d) Scatterplot of the interaction between the cued recall index and connectivity loadings of the cluster depicted in (c) and grouped by resting state sessions. (e) Sagittal image of the session × performance interaction located in BA9 with the baseline Visual circuit. (f) Scatterplot of the interaction between the cued recall index and connectivity loadings extracted from the cluster depicted in (e) and grouped by resting state sessions. (g) Axial image of the session × performance interaction located in the right thalamus within the post-encoding Executive control circuit. (h) Scatterplot of the interaction between the cued recall index and connectivity loadings extracted from the cluster depicted in (g) and grouped by resting state sessions. (i) Axial image of the session × performance interaction located in the right parahippocampal gyrus with the post-encoding Primary visual circuit. (j) Scatterplot of the interaction between the cued recall index and connectivity loadings extracted from the cluster depicted in (i) and grouped by resting state sessions. (k) Sagittal image of the session × performance interaction located in BA10 with the post-encoding Primary visual circuit. (l) Scatterplot of the interaction between the cued recall index and connectivity loadings extracted from the cluster depicted in (k) and grouped by resting state sessions. All results are defined at TFCE-FWE $p<0.05$. Abbreviations: COI=Component of Interest; the apex 'b' refers to baseline extracted COIs, while apex 'p' refers to post-encoding extracted COIs; IC= Independent component; BA=Brodmann Area; *L*=left; *R*=right; *C*= brain-circuits.

Pergola et al., 2013). Reaction time analysis suggested faster novelty detection than recognition (Bowman and Dennis, 2016). Subsequent memory effects were significantly above chance level.

4.2. Preserved and reconfigured brain circuits

We found that resting state system configuration is not fixed, but rather varies in a short time span following cognitive task engagement – in this case, tapping into episodic memory. We captured both persistence and changes of brain circuits between baseline and post-encoding resting state, suggesting that the interposed exposure to the episodic memory task may be associated with changes in terms of overall brain functional configuration.

As the FC configuration within executive control, default mode, and cerebellar circuits persisted from baseline to post-encoding, our findings show an overall stability of these circuits during resting state in the experimental design we employed, perhaps reflecting a stable intrinsic framework during resting state. Particularly, individual FC loadings within the executive control circuit during both baseline and post-encoding were associated with individual memory performance, thus suggesting that executive control circuit persistence is possibly instrumental to memory processes (Cole et al., 2013; Raichle, 2015; Sambataro et al., 2010b, 2012).

On the other hand, the lower degree of overlap between visual circuits from baseline to post-encoding resting state suggests a functional reorganization shortly after the memory task. Notably, individual FC loadings during baseline within the visual circuit were not associated with memory performance, whereas the same measure in both the reconfigured visual circuits correlated with memory performance during post-encoding. This association suggests an instrumental role of the reconfiguration of the visual circuit for the subsequent retrieval of the encoded memories. Prior evidence identified early memory-dependent microstructural changes along the dorsal and ventral visual pathways (Brodt et al., 2018) and FC changes of these areas in relation with MTL activity in an ROI-selective analysis (Tambini et al., 2010). Here, we show that the previously reported region-specific changes may be integrated in a system perspective: FC configuration changes affect visual cortex functional interplay with the MTL and PFC, highlighting a wider

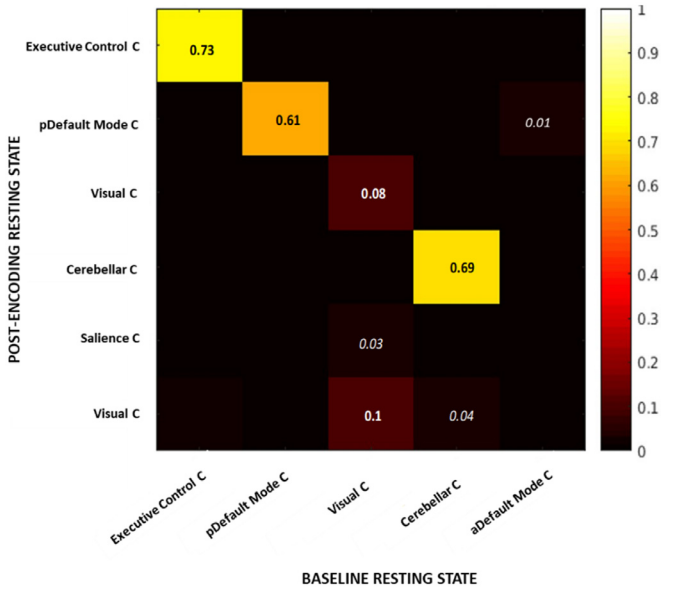

Fig. 5. Heatmap showing the association between baseline resting state estimated COIs and post-encoding resting state estimated COIs. R-squared are reported. Abbreviations: *a* = anterior; *p* = posterior; *C* = brain-circuits.

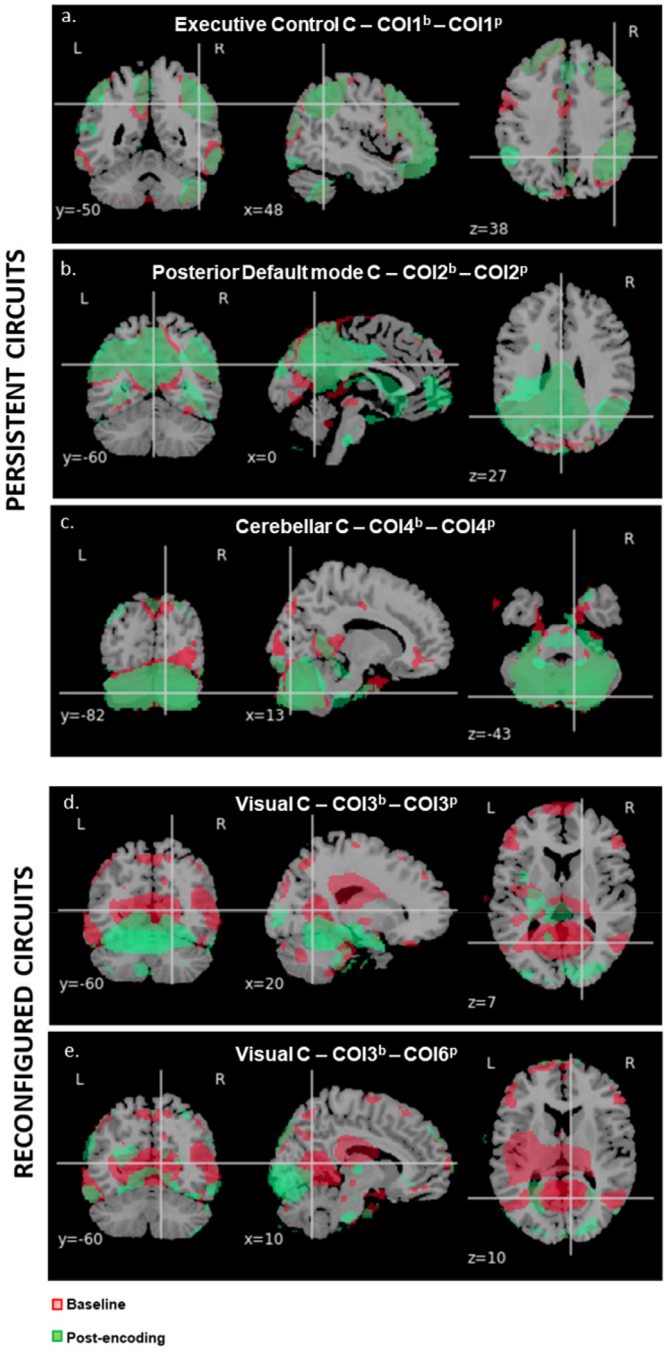

Fig. 6. Sections showing the spatial overlap between persistent circuits, i.e., a) the baseline and post-encoding executive control circuits (COI1^b and COI1^p); b) the baseline and post-encoding posterior default mode circuits (COI2^b and COI2^p); c) and the baseline and post-encoding cerebellar circuits (COI4^b and COI4^p); and reconfigured circuits, i.e., d) the baseline visual circuit and the post-encoding cerebellar-visual circuit (COI3^b and COI3^p); e) the baseline and the post-encoding visual circuits (COI3^b and COI6^p).

flexible mechanism shortly after performance of an episodic memory task, while early processing of memories is taking place.

A caution against over-interpreting the functional significance of these findings derives from two aspects. First, we could not determine the causal relationships between preserved and reconfigured circuits, i.e., whether undetected between-circuit relationships are associated with memory performance. For example, visual circuit changes may be related to its connectivity with executive or default mode circuits even though we have not found changes within these circuits. Establishing causality in this preservation and reconfiguration scenario is especially intriguing to investigate the neural basis of individual memory ability. Second, it should be taken into consideration that the failure to replicate the anterior default mode circuit and the salience circuit across sessions may relate with our strict pruning criteria for IC selection, which were based on high quality and stability of correlated signal across regions (Supplementary materials, Section 7). In other words, we cannot infer that the anterior default mode is not active during post-encoding, and the salience circuit is not active during baseline. Rather, their related circuits properties were characterized by low internal stability, thus preventing the possibility to be reliably extracted at a higher level of granularity.

Despite these cautions, it should be noted that the forward/backward strategy we employed does not entail identifying a single connectivity model across sessions (as is the case for standard multiple-session ICA), but rather measures FC changes from a bi-directional temporal perspective. The advantage of such bi-directional FC approach is that it allowed us to characterize the involvement of known memory key regions (i.e., MTL, PFC, and thalamus) in the process of learning through the investigation of FC changes between these localized regions and whole-brain multiple-session system configuration changes occurring shortly after learning. Notably, these local and system-level changes occurred in absence of rehearsal and long-time spans, thus supporting the notion that the process of learning is paralleled by brain functional connectivity changes already few minutes after the learning experience.

4.3. Localized dynamics associated with system-level FC reconfiguration support memory performance

Our system perspective has been enriched by the definition of the regional involvement of memory key regions, whose FC resulted flexible as well. As outlined above, previous evidence for such involvement came from ROI-based approaches showing local changes in terms of connectivity between the aforementioned regions (Brodt et al., 2018; Tambini et al., 2010; Wagner et al., 2019). Notably, our ICA procedure can parse signal from one region into multiple functional components, therefore identifying different patterns relative to correlations between time series.

In detail, we have found PFC FC localized changes in interaction with the visual circuit reconfiguration, such that PFC resulted connected with visual cortex both during baseline and post-encoding resting state, and best performers had increased FC. An interpretation of this result may be that PFC connectivity with visual cortex supports both the successful encoding and the following post-encoding processing of memories. Thus, we may speculate that the engagement of fronto-parietal cortices promotes the early processing of memories not requiring rehearsal or long delay period after the learning experience (Tambini and Davachi, 2019).

On the other side, we found that the MTL FC with visual circuits appeared inverted between baseline and post-encoding resting state, showing FC flexibility also at the regional level. Tambini et al. (2010) found that MTL FC with occipital regions increased during post-encoding resting state and was associated with memory performance. Here, we found an opposite correlation between MTL FC with visual circuit and memory performance. A possible interpretation is that tight coupling within this visual circuit antagonized memory performance, and the MTL of best performers tended to disengage from this connectivity pattern. Consistently, previous literature showed that memory key regions change their role and prominence within FC patterns already shortly after the encoding. For example, Brodt et al. (2018) reported microstructural changes in terms of decreased connections between MTL and neocortex associated with memory performance already one hour after learning. The authors hypothesized that this anatomical MTL-neocortex interplay might support early processing of memories. Our results support this view from a functional perspective, suggesting an even earlier functional MTL-neocortex interplay underlying the processing of memories. Future studies aimed at understanding the FC configurational changes from the post-encoding phase to the completion of the consolidation process are warranted to fully characterize brain system changes supporting the consolidation of memory traces.

Furthermore, our results showed that thalamic FC within the executive control circuit varied across sessions as a function of individual memory performance. Right thalamic FC was negatively associated with memory performance during baseline and positively during post-encoding. These findings are consistent with proposed hypotheses that the thalamus enhances the efficiency of cortical circuits during high cognitive demand and updating operations, potentially via the regulation of cognition-related PFC regions of the executive control circuit (Antonucci et al., 2021; Halassa and Sherman, 2019; Mitchell, 2015; Pergola et al., 2018). Specifically, this balance between the thalamic disengagement with fronto-parietal regions during baseline and the thalamic engagement with fronto-parietal regions after the encoding seems to be instrumental to learning success.

Notably, Wagner et al. (2019) showed increased anterior and mediodorsal thalamic coupling with PFC and MTL, as well as an increased medioventral and lateral dorsal thalamic coupling with posterior parietal and posterior medial cortex, as a function of individual performance. The authors suggested a model in which the crosstalk between thalamic subdivisions, MTL, PFC and posterior cortices supports long-term memory stabilization. Our results support this previous evidence, however, future studies are warranted to further investigate the specificity of each thalamic subdivision, as well as thalamo-cortical connections in memory processes.

4.4. Limitations

The present study was conducted on a relatively small cohort and the configuration changes detected were not externally replicated in other geographically diverse datasets acquired on different scanners. Our focus was on FC changes at the whole-brain level shortly after the exposure to a learning experience, thus it remains to be addressed how these functional changes are associated with long-term consolidation of memories. Moreover, it should be considered that our episodic memory task included multiple phases - encoding, delay, retrieval. This design makes it difficult to disentangle which phase underlies the changes we detected between baseline and post-encoding resting state.

From the methodological perspective, it should be also taken into account that our ICA separation procedure led to the aggregation of several functional circuits, possibly separated with better powered and more granular analyses, into the same IC, as we estimated few ICs aimed at reflecting wider and more functionally coherent circuits (Iraji et al., 2019).

Conclusions

In this study, we showed that the overall configuration of the human brain changes shortly after a learning experience, and we suggest that this reconfiguration process is instrumental to memory performance. We found both system persistence, with respect to the default mode, cerebellar, and executive control circuits, and reconfiguration, related to the visual circuit, across sessions. Furthermore, our findings show a high degree of inter-individual variability across sessions in terms of FC changes between memory key regions - including MTL, PFC, visual cortices, and thalamus - and the executive control circuit, as a function of the memory performance. These results further define the pivotal role of such regions and circuits in memory processes, as well as their high degree of flexibility related to memory processes. Overall, we offer a broader perspective on functional and spatially distributed brain system configuration which support memory and provide a deeper understanding of early-stage FC pattern changes associated with the heterogeneity of memory performance across individuals.

Data and code availability statement

Due to the nature of this research, participants of this study did not agree for their data to be shared publicly, so supporting data is not available.

Declaration of Competing Interest

Alessandro Bertolino received consulting fees by Biogen and lecture fees by Otsuka, Janssen, Lundbeck. All other authors have no biomedical financial interests and no potential conflicts of interest.

Credit authorship contribution statement

Roberta Passiatore: Formal analysis, Methodology, Writing – original draft, Visualization. **Linda A. Antonucci:** Conceptualization, Methodology, Writing – original draft, Supervision. **Sabine Bierstedt:** Investigation. **Manojkumar Saranathan:** Software. **Alessandro Bertolino:** Writing – review & editing, Funding acquisition, Resources. **Boris Suchan:** Investigation, Data curation, Project administration, Funding acquisition, Writing – review & editing, Resources. **Giulio Pergola:** Conceptualization, Investigation, Data curation, Project administration, Funding acquisition, Writing – original draft, Supervision.

Acknowledgments

Giulio Pergola has received a travel award for an academic exchange program from the non-profit organization Boehringer Ingelheim Fonds leading to this work. Boris Suchan was funded by a grant covering scan acquisition costs (Sonderforschungsbereich 874, CRC 874) from the German Research Foundation (Deutsche Forschungsgemeinschaft, DFG, Project B8). We thank Philips Germany, especially Burkhard Maedler for continuous scientific support. Roberta Passiatore's scholarship was funded by a Collaboration Grant from Exprivia SpA, awarded to Alessandro Bertolino. Linda A. Antonucci's position was funded by the Structural European Funding of the Italian Minister of Education (Attraction and International Mobility—AIM—action, Grant No. 1859959). We would also like to thank Rita Cosoli, Grazia Difonzo, Dr. Leonardo Fazio,

Valentina Felici, Christine Huecke, Dr. Robert Lech, Dr. Alfonso Monaco, Monica Nicoli, and Nora Penzel for their help at different stages of this research.

References

Allen, E.A., Erhardt, E.B., Damaraju, E., Gruner, W., Segall, J.M., Silva, R.F., Havlicek, M., Rachakonda, S., Fries, J., Kalyanam, R., Michael, A.M., Caprihan, A., Turner, J.A., Eichele, T., Adelsheim, S., Bryan, A.D., Bustillo, J., Clark, V.P., Feldstein Ewing, S.W., Filbey, F., Ford, C.C., Hutchison, K., Jung, R.E., Kiehl, K.A., Kodituwakku, P., Komesu, Y.M., Mayer, A.R., Pearlson, G.D., Phillips, J.P., Sadek, J.R., Stevens, M., Teuscher, U., Thoma, R.J., Calhoun, V.D., 2011. A baseline for the multivariate comparison of resting-state networks. Front. Syst. Neurosci. 5, 2.

Alvarez, P., Squire, L.R., 1994. Memory consolidation and the medial temporal lobe: a simple network model. Proc. Natl. Acad. Sci. U. S. A. 91, 7041–7045.

Antonucci, L.A., Di Carlo, P., Passiatore, R., Papalino, M., Monda, A., Amoroso, N., Tangaro, S., Taurisano, P., Rampino, A., Sambataro, F., Popolizio, T., Bertolino, A., Pergola, G., Blasi, G., 2019. Thalamic connectivity measured with fMRI is associated with a polygenic index predicting thalamo-prefrontal gene co-expression. Brain Struct. Funct..

Antonucci, L.A., Penzel, N., Pigoni, A., Dominke, C., Kambeitz, J., Pergola, G., 2021. Flexible and specific contributions of thalamic subdivisions to human cognition. Neurosci. Biobehav. Rev..

Antonucci, L.A., Taurisano, P., Fazio, L., Gelao, B., Romano, R., Quarto, T., Porcelli, A., Mancini, M., Di Giorgio, A., Caforio, G., Pergola, G., Popolizio, T., Bertolino, A., Blasi, G., 2016. Association of familial risk for schizophrenia with thalamic and medial prefrontal functional connectivity during attentional control. Schizophr. Res. 173, 23–29.

Avants, B.B., Tustison, N., Song, G., 2009. Advanced normalization tools (ANTS). Insight J. 2, 1–35.

Bassett, D.S., Wymbs, N.F., Porter, M.A., Mucha, P.J., Carlson, J.M., Grafton, S.T., 2011. Dynamic reconfiguration of human brain networks during learning. Proc. Natl. Acad. Sci. U. S. A. 108, 7641–7646.

Bowman, C.R., Dennis, N.A., 2016. The neural basis of recollection rejection: increases in hippocampal-prefrontal connectivity in the absence of a shared recall-to-reject and target recollection network. J. Cogn. Neurosci. 28, 1194–1209.

Brodt, S., Gais, S., Beck, J., Erb, M., Scheffler, K., Schönauer, M., 2018. Fast track to the neocortex: a memory engram in the posterior parietal cortex. Science 362, 1045–1048.

Calhoun, V.D., Adali, T., Pearlson, G.D., Pekar, J.J., 2001. A method for making group inferences from functional MRI data using independent component analysis. Hum. Brain Mapp. 14, 140–151.

Cohen, J.R., D'Esposito, M., 2016. The segregation and integration of distinct brain networks and their relationship to cognition. J. Neurosci. 36, 12083–12094.

Cole, M.W., Bassett, D.S., Power, J.D., Braver, T.S., Petersen, S.E., 2014. Intrinsic and task-evoked network architectures of the human brain. NeuronNeuron 83, 238–251.

Cole, M.W., Reynolds, J.R., Power, J.D., Repovs, G., Anticevic, A., Braver, T.S., 2013. Multi-task connectivity reveals flexible hubs for adaptive task control. Nat. Neurosci. 16, 1348–1355.

Damoiseaux, J.S., Rombouts, S.A., Barkhof, F., Scheltens, P., Stam, C.J., Smith, S.M., Beckmann, C.F., 2006. Consistent resting-state networks across healthy subjects. Proc. Natl. Acad. Sci. U. S. A. 103, 13848–13853.

Dewhurst, S.A., Holmes, S.J., Brandt, K.R., Dean, G.M., 2006. Measuring the speed of the conscious components of recognition memory: remembering is faster than knowing. Conscious. Cogn. 15, 147–162.

Du, Y., Fan, Y., 2013. Group information guided ICA for fMRI data analysis. Neuroimage 69, 157–197.

Dudai, Y., 2004. The neurobiology of consolidations, or, how stable is the engram? Annu. Rev. Psychol. 55, 51–86.

Dudai, Y., Karni, A., Born, J., 2015. The Consolidation and Transformation of Memory. NeuronNeuron 88, 20–32.

Ferrucci, R., Brunoni, A.R., Parazzini, M., Vergari, M., Rossi, E., Fumagalli, M., Mameli, F., Rosa, M., Giannicola, G., Zago, S., Priori, A., 2013. Modulating human procedural learning by cerebellar transcranial direct current stimulation. Cerebellum 12, 485–492.

Frankland, P.W., Bontempi, B., 2005. The organization of recent and remote memories. Nat. Rev. Neurosci. 6, 119–130.

Friston, K., 2003. Learning and inference in the brain. Neural Netw. 16, 1325–1352.

Greicius, M.D., Krasnow, B., Reiss, A.L., Menon, V., 2003. Functional connectivity in the resting brain: a network analysis of the default mode hypothesis. Proc. Natl. Acad. Sci. U. S. A. 100, 253–258.

Halassa, M.M., Sherman, S.M., 2019. Thalamocortical circuit motifs: a general framework. NeuronNeuron 103, 762–770.

Himberg, J., Hyvarinen, A., Esposito, F., 2004. Validating the independent components of neuroimaging time series via clustering and visualization. NeuroimageNeuroimage 22, 1214–1222.

Hyvarinen, A., 1999. Fast and robust fixed-point algorithms for independent component analysis. Ieee Trans. Neural Netw. 10, 626–634.

Iraji, A., Deramus, T.P., Lewis, N., Yaesoubi, M., Stephen, J.M., Erhardt, E., Belger, A., Ford, J.M., McEwen, S., Mathalon, D.H., Mueller, B.A., Pearlson, G.D., Potkin, S.G., Preda, A., Turner, J.A., Vaidya, J.G., van Erp, T.G.M., Calhoun, V.D., 2019. The spatial chronnectome reveals a dynamic interplay between functional segregation and integration. Hum. Brain Mapp. 40, 3058–3077.

Jeong, W., Chung, C.K., Kim, J.S., 2015. Episodic memory in aspects of large-scale brain networks. Front. Hum. Neurosci. 9, 454.

Kareev, Y., Trope, Y., 2011. Correct acceptance weighs more than correct rejection: a decision bias induced by question framing. Psychon. Bull. Rev. 18, 103–109.

Kim, D.I., Manoach, D.S., Mathalon, D.H., Turner, J.A., Mannell, M., Brown, G.G., Ford, J.M., Gollub, R.L., White, T., Wible, C., Belger, A., Bockholt, H.J., Clark, V.P., Lauriello, J., O'Leary, D., Mueller, B.A., Lim, K.O., Andreasen, N., Potkin, S.G., Calhoun, V.D., 2009. Dysregulation of working memory and default-mode networks in schizophrenia using independent component analysis, an fBIRN and MCIC study. Hum. Brain Mapp. 30, 3795–3811.

Ma, S., Correa, N.M., Li, X.L., Eichele, T., Calhoun, V.D., Adali, T., 2011. Automatic identification of functional clusters in FMRI data using spatial dependence. IEEE Trans. Biomed. Eng. 58, 3406–3417.

Mitchell, A.S., 2015. The mediodorsal thalamus as a higher order thalamic relay nucleus important for learning and decision-making. Neurosci. Biobehav. Rev. 54, 76–88.

Moscovitch, M., Cabeza, R., Winocur, G., Nadel, L., 2016. Episodic memory and beyond: the hippocampus and neocortex in transformation. Annu. Rev. Psychol. 67, 105–134.

Nadel, L., Moscovitch, M., 1997. Memory consolidation, retrograde amnesia and the hippocampal complex. Curr. Opin. Neurobiol. 7, 217–227.

Oldfield, R.C., 1971. The assessment and analysis of handedness: the Edinburgh inventory. Neuropsychologia 9, 97–113.

Olsen, R.K., Robin, J., 2020. Zooming in and zooming out: the importance of precise anatomical characterization and broader network understanding of MRI data in human memory experiments. Curr. Opin. Behav. Sci. 32, 57–64.

Pergola, G., Danet, L., Pitel, A.L., Carlesimo, G.A., Segobin, S., Pariente, J., Suchan, B., Mitchell, A.S., Barbeau, E.J., 2018. The regulatory role of the human mediodorsal thalamus. Trends Cogn. Sci. 22, 1011–1025.

Pergola, G., Gunturkun, O., Koch, B., Schwarz, M., Daum, I., Suchan, B., 2012. Recall deficits in stroke patients with thalamic lesions covary with damage to the parvocellular mediodorsal nucleus of the thalamus. Neuropsychologia 50, 2477–2491.

Pergola, G., Ranft, A., Mathias, K., Suchan, B., 2013. The role of the thalamic nuclei in recognition memory accompanied by recall during encoding and retrieval: an fMRI study. Neuroimage 74, 195–208.

Pergola, G., Suchan, B., 2013. Associative learning beyond the medial temporal lobe: many actors on the memory stage. Front. Behav. Neurosci. 7, 162.

Power, J.D., Barnes, K.A., Snyder, A.Z., Schlaggar, B.L., Petersen, S.E., 2012. Spurious but systematic correlations in functional connectivity MRI networks arise from subject motion. Neuroimage 59, 2142–2154.

Raichle, M.E., 2015. The brain's default mode network. Annu. Rev. Neurosci. 38, 433–447.

Sambataro, F., Blasi, G., Fazio, L., Caforio, G., Taurisano, P., Romano, R., Di Giorgio, A., Gelao, B., Lo Bianco, L., Papazacharias, A., Popolizio, T., Nardini, M., Bertolino, A., 2010a. Treatment with olanzapine is associated with modulation of the default mode network in patients with Schizophrenia. Neuropsychopharmacology 35, 904–912.

Sambataro, F., Murty, V.P., Callicott, J.H., Tan, H.Y., Das, S., Weinberger, D.R., Mattay, V.S., 2010b. Age-related alterations in default mode network: impact on working memory performance. Neurobiol. Aging 31, 839–852.

Sambataro, F., Safrin, M., Lemaitre, H.S., Steele, S.U., Das, S.B., Callicott, J.H., Weinberger, D.R., Mattay, V.S., 2012. Normal aging modulates prefrontoparietal networks underlying multiple memory processes. Eur. J. Neurosci. 36, 3559–3567.

Stark, C.E., Squire, L.R., 2001. When zero is not zero: the problem of ambiguous baseline conditions in fMRI. Proc. Natl. Acad. Sci. U. S. A. 98, 12760–12766.

Tambini, A., Davachi, L., 2019. Awake reactivation of prior experiences consolidates memories and biases cognition. Trends Cogn. Sci. 23, 876–890.

Tambini, A., Ketz, N., Davachi, L., 2010. Enhanced brain correlations during rest are related to memory for recent experiences. Neuron 65, 280–290.

Wagner, I.C., van Buuren, M., Fernández, G., 2019. Thalamo-cortical coupling during encoding and consolidation is linked to durable memory formation. Neuroimage 197, 80–92.

Yue, Q., Martin, R.C., Fischer-Baum, S., Ramos-Nunez, A.I., Ye, F., Deem, M.W., 2017. Brain modularity mediates the relation between task complexity and performance. J. Cogn. Neurosci. 29, 1532–1546.